A UV laser test facility for precise measurement of gas parameters in gaseous detectors

Fan, X.; Naumann, L.; Siebold, M.; Stach, D.; Kämpfer, B.;

Originally published:

December 2020

Nuclear Instruments and Methods in Physics Research A 988(2021), 164929

DOI: https://doi.org/10.1016/j.nima.2020.164929

Perma-Link to Publication Repository of HZDR:

https://www.hzdr.de/publications/Publ-31902

A UV laser test facility for precise measurement of gas parameters in gaseous detectors

X. Fan[1], L. Naumann[1], M. Siebold[1], D. Stach[1], and B. Kämpfer[1]

[1]Helmholtz-Zentrum Dresden-Rossendorf (HZDR), Dresden, Germany

November 20, 2020

Abstract

This work is devoted to the development of a UV laser test facility for calibration of gaseous detectors. We applied multiple methods to achieve a micrometer scale accuracy for the laser test facility and provide dedicated investigations for laser ionization in the gaseous detector. With the well-controlled laser ionization and remote DAQ system, we can operate the calibration of gaseous detectors and precise measurement of gas parameters at the micrometer scale related to the detector's field geometry.

1 Introduction

Researchers have been using pulsed UV laser in the calibration for gaseous detectors and the measurement of gas parameters in many works. The early applications [1–4] showed that laser ionization could be applied in different gas mixtures with very stable performance. Therefore, dedicated researches are carried out for the in-depth understanding of laser ionization in wire detectors [5, 6], and later on in other detectors like Resistive Plate Chamber (RPC) [7, 8]. The laser test method can provide very high spatial accuracy because the working gas inside the detector is ionized by Multi-photon Ionization (MPI) effect at the micrometer scale within the laser focus.

Despite the achievements in detectors with larger gas volume, the application of the laser ionization method in the micrometer scale is yet to be achieved, due to the difficulty of laser alignment and the complexity of the positioning system. Based on the previous understandings, we believe that increasing the order of overall accuracy can be achieved by combining multiple methods.

This paper reports a high accuracy laser test facility assembled in HZDR, based on the facility reported in [9]. The test facility includes a picosecond UV laser pulse generator, a drift tube detector with micrometer accuracy moving stage, and a remote DAQ system. A dedicated investigation of the laser ionization process in a gaseous detector is performed.

2 Laser test facility setup

2.1 Pulse generation and focusing

Picosecond laser pulses are generated in a Master Oscillator Power Amplifier (MOPA) operating

at a center wavelength of 1030 nm. A commercial mode-locked fiber oscillator with a repetition rate of 20 MHz and a pulse duration of 10 ps is employed as seed source. A maximum output pulse energy of 1 µJ and a pulse duration of 2 ps are achieved with a regenerative Yb:YAG amplifier similar to [10]. Its repetition rate can be adjusted within a wide range from 0 to 100 kHz using a BBO Pockels cell. Second (515 nm) and fourth harmonic (257.5 nm) radiation is generated in a RTP and a BBO crytsal at an efficiency of around 10%.

Two remote controlled attenuator wheels are used to adjust the beam intensity for the described application. Afterwards, the laser is focused by an optical system consisting of three lenses with focal length of 5 cm, 5 cm and 1.5 cm, respectively. Two apertures are installed for laser beam alignment. A schematic drawing of the optical system is shown in Figure 1.

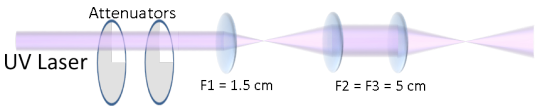

Figure 1: The optical system for laser focusing.

2.2 Mechanical system with automatic program

A mechanical platform with an automatic controlling system is used for the tests.

In the experiments, a detector box or a sharp edge is mounted on a high accuracy 3-dimension moving stage (OWIS Motorized XYZ Stage KTM 65). The step length of the moving stage is set to 1 µm with the accuracy better than 5 nm.

The multi-function control and analysis program are written with Labview [11]. It provides the functions to proceed with automatic long term, high precision scanning and data taking. When the detector box or the sharp edge is mounted, the moving stage will move to the position given by the program, so that the relative position of the laser focus to the detector or the edge is changed.

The detector signals are monitored by an oscilloscope (Lecroy Waverunner 640zi). The waveforms are stored and analyzed off-line, where time-over-threshold, charge, and amplitude of each waveform are obtained.

2.3 The drift tube detector

The drift tube is considered as an appropriate detector for laser-induced plasma calibration. It works in the proportional mode so that the signal charge of the detector depends on the working condition of the detector and the initial number of primary electrons. The drift tube has a large volume as its drift zone and the drift length is up to 6 mm long, and the signal charge is independent on the laser focus position inside the active gas volume. Besides, the drift tube is a well-studied detector with simple electric field distribution and high working stability.

We designed a drift tube detector mounted inside an aluminium gas box for this experiment. The gas box has two windows made from quartz glass with anti-reflection coating for light input and output. One glass window can be replaced by a 0.05 mm thin Kapton foil (polymide) to allow X-rays to pass through in the tests with ^{55}Fe source. The aluminium box has gas tightness and high mechanical precision.

The drift tube has two tangential slits for laser beam passage. The tube is gold-plated to prevent the photoelectric effect on the inner cathode surface while providing chemical and thermal stability. The inner radius of the cathode tube is 6 mm. The drift tube detector's anode is a Tungsten wire of 6 µm diameter in the centre of the cathode tube. The working gas is 70% Ar + 30% CO_2 with the flush rate of 10 mL/min at atmospheric pressure and room temperature.

The signal is read out from the anode wire. The anode wire is connected via an RC-splitter box to a pre-amplifier with the gain of 43 dB. The trigger signal for the oscilloscope is taken from a laser diode inside the laser generation sys-

tem to provide a precise starting time. The time resolution is better than a picosecond. Then the amplified signal is fed into the oscilloscope.

3 Experiments

3.1 Simulation of Laser Ionization

A laser focus from uniform laser beam can be described by gaussian beam. The laser intensity is described as:

$$I(r,z) = \frac{P}{\pi\, w(z)^2} e^{\left(-2\frac{r^2}{w(z)^2}\right)} , \tag{1}$$

$$w(z) = w_0 \sqrt{1 + \left(\frac{z}{Z_R}\right)^2} , \tag{2}$$

$$Z_R = \frac{\pi\, w_0^2}{\lambda} , \tag{3}$$

$$w_0 = \frac{\lambda}{\pi\, \theta} , \tag{4}$$

where P is the total power of laser, r and z describes the polar coordinates position, $I(r,z)$ is the laser intensity, $w(z)$ is the beam radius, w_0 is the beam waist (minimum beam radius), Z_R is the Rayleigh length, λ is the wavelength and θ is the beam angle.

When a photon's energy is below the ionization potential of particles, the photoelectric effect does not happen. However, when the laser energy is beyond a threshold value, the MPI effect can be observed. During the process, the particle will absorb several photons until the particle is ionized.

In this work, the laser intensity is around $10 \times 10^{10}\,\mathrm{W/cm^2}$ so that the ionization is only ignited by the MPI effect and not by other effects. As the photons are absorbed sequentially in MPI, the cross-section σ_{MPI} absorbing $\langle n \rangle$ photons can be written as:

$$\sigma_{MPI} = \sigma_{0to1} \cdot \sigma_{1to2} \ldots \sigma_{<n-1>to\langle n \rangle} . \tag{5}$$

The number of electrons is:

$$N_e = \sigma_{MPI} I^{\langle n \rangle} , \tag{6}$$

where I is the laser intensity. The number $\langle n \rangle$ is the MPI power.

As the beam radius is small, we can first calculate the one-dimension electron distribution along the laser beam axis Z. From Equation 1 and Equation 6, the number of electrons ionized along the laser beam axis Z is:

$$\begin{aligned} N_e(z) &= \int_{\theta=0}^{\theta=2\pi} \int_{r=0}^{r=\infty} N_e(z,r) r dr d\theta \quad (7) \\ &= 2\pi \int_{r=0}^{r=\infty} N_e(z,r) r dr \quad (8) \\ &= C \left(\frac{1}{1 + \left(\frac{z}{Z_R}\right)^2} \right)^{\langle n \rangle - 1} , \quad (9) \end{aligned}$$

where C is a constant related to P, w_0 and $\langle n \rangle$. Then the FWHM of the one-dimension electron distribution can be calculated as:

$$N_e(Z_{half}) = C \left(\frac{1}{1+\left(\frac{Z_{half}}{Z_R}\right)^2} \right)^{\langle n \rangle - 1} \tag{10}$$

$$\left(\frac{1}{1+\left(\frac{Z_{half}}{Z_R}\right)^2} \right)^{\langle n \rangle - 1} = \frac{1}{2} \tag{11}$$

$$Z_{half} = Z_R \sqrt{\sqrt[\langle n \rangle - 1]{2} - 1} . \tag{12}$$

It is obtained in Section 3.4 that the MPI power amounts $\langle n \rangle = 2$ in the experiments. As a result, the electron distribution becomes a Lorentz function (Cauchy function), so that $Z_{half} = Z_R$, the FWHM of the electron Z distribution, is equal to two times the Rayleigh length Z_R.

A simulation program is established based on Equation 1 and Equation 6. It divides the given space surrounding the laser focus into tiny elements and calculates the value at its center. The values can be integrated to calculate the distribution of laser intensity or electron ionization number. The 1D results presented in Figure 2 from simulation and from Equation 12 are in agreement. It can be concluded that the majority

number of electrons are distributed in a small area. It also shows that the beam angle θ and the MPI power $\langle n \rangle$ have a strong influence on the distribution area, where larger θ and higher $\langle n \rangle$ make the ionizations more focused.

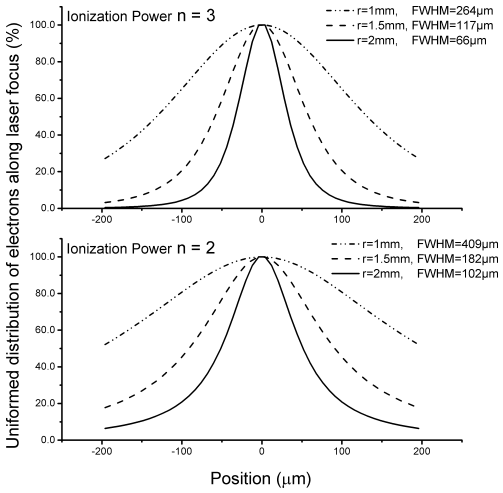

Figure 2: The distribution of number of electron along the laser beam, where n is the MPI power, r is the beam radius at the lens, as the focus length of the lens is 50 mm, so that the beam angle is $\theta = \frac{r}{50mm}$.

An electron distribution in 2D projection is presented in Section 3.2 and will be further discussed.

3.2 Imaging of laser focus

A scalpel is mounted on the moving stage as an edge to shield part of the laser beam to image the intensity distribution in the laser focus area. The energy of the unshielded part of the laser is measured by a laser power meter (OPHIR VEGA).

When the edge is placed at different positions in a section perpendicular to the laser beam direction, the laser beam intensity from zero to maximum value will be acquired, depending on the shielded laser beam fraction. The laser energy within two positions is the difference between the two positions' measurement value, and finally, the laser intensity distribution along the section is obtained.

A row of sections perpendicular to the laser beam with a fixed distance is defined by the automatic step-scanning program. The laser energies are measured when the edge is scanned with a defined step length on the sections. The distributions along all the sections are combined into a 2D figure as the projection distribution of the laser intensity, as shown in Figure 3.

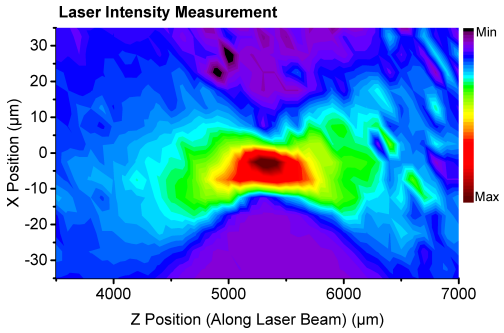

Figure 3: The laser intensity distribution where the beam angle is $\theta = \frac{1mm}{50mm}$.

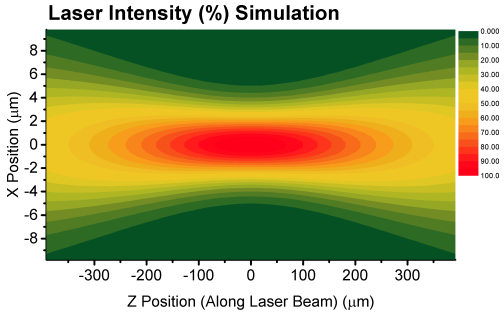

Figure 4: The laser intensity distribution calculated using same parameters in Figure 3.

It can be concluded from Figure 3 that at the waist of the focus, the beam radius amounts 5 μm and the FWHM length of the focus is approximately 400 to 500 μm. It is in agreement with the

calculation using the parameters obtained from experiments, shown in Figure 4.

3.3 Number of electrons in primary ionizations

To calibrate the initial number of primary electrons in an avalanche by laser ionization, the gas ionization by 5.9 keV X-rays from a ^{55}Fe radiation source is used for comparison. During the experiment, one of the quartz laser windows is replaced by a thin Kapton foil to allow the X-rays to pass through. The ^{55}Fe source is placed close to the window to obtain a maximum counting rate.

The activity of the ^{55}Fe source is approximately 4×10^5 Bq. When a particle of the working gas in the drift tube absorbs a photon from a radiation source, an electron-ion pair is produced. The escaped electron will ionize other gas molecules. The average ionization energy to produce one electron-ion pair is 26 eV for Argon and 33 eV for CO_2, respectively. A total number of approximately 200 electrons within a small volume is expected from a photon emitted from a ^{55}Fe source. The calibration has been provided with different high voltages.

A Monte-Carlo simulation program based on Magboltz is developed to study the ionization process as well. From the simulation, it is observed that the process of energy loss is within a relatively tiny volume with the dimension of several micrometers The distribution of signal charges from the drift tube is expected to be independent of the primary ionization position.

The laser experiments are operated in a similar way, where the UV-anti reflection quartz glass is assembled. The attenuators (Continuously Variable Metallic Neutral Density Filters) between the laser generator and optical system are set to different attenuation rates to change the laser energy. The laser focus is placed at the position of 1500 µm from the wire. The same working voltages for the drift tube, applied for ^{55}Fe source test are also applied in the laser test.

The results from the tests are shown in Figure 5. It can be observed that the primary number of electrons by X-rays from ^{55}Fe source and by 1.6×10^{10} W/cm^2 laser is comparable in the specific experimental condition of the calibration test. Also, the charge dependence on the primary ionization is supported by the results.

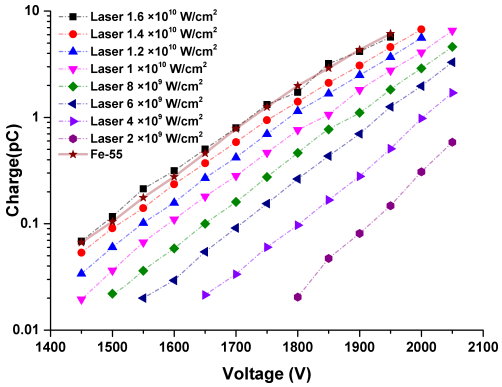

Figure 5: The charges of signals generated by laser and by ^{55}Fe source in the drift chamber detector in dependence on the anode voltage and laser intensities. The laser intensity is the average laser intensity at the section of beam waist.

3.4 Measurement of Multi-Photon Ionization power

The MPI power is one of the main parameters in the laser ionization process.

A precise measurement of MPI power is essential for understanding the laser ionization in the specific experimental conditions.

The photon energy of the laser is 4.82 eV, and the ionization potential (minimum energy for ionization) of Argon and CO_2 are 15.7 eV and 14.4 eV, respectively. As a result, 4 or 3 photons should be absorbed during the excitation time to ionize an Argon or a CO_2 particle, respectively. If the laser ionization is from the gas mixture, it is expected that the MPI power is 3. However, according to the research result in [6] that the ionization is mainly from the gas impurities

with low ionization potential; if this is the case, then the MPI power is 2. It is necessary to carry out the measurement results at high accuracy to clarify the following questions: what portion is the main contribution to the ionization process and whether the MPI power values are integers or continuous numbers.

One attenuator is mounted on a high precision rotation stage (OWIS PS10), the Labview program controls the stage. The accuracy of the degree is controlled to 0.1°, and the accuracy of the laser intensity is 0.2%. The laser point is placed at a position 1000 µm from the anode wire. The signal charges are obtained for different laser intensities. The experimental results are shown in Figure 6. By linear fit under logarithmic coordinates, the MPI power is obtained as 2.007 ± 0.035.

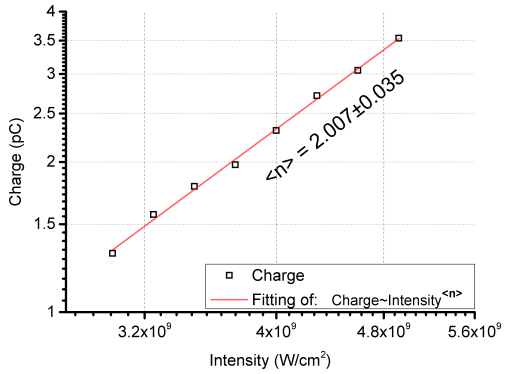

Figure 6: The average signal charge of the drift tube in dependence on the laser intensity in double log scale.

It can be concluded that in our experiments with the drift tube detector for the laser test facility, the ionization does not come from the working gases, but from impurities with lower ionization potentials, as reported in [6].

3.5 Measurement of gas parameters

As the drift chamber detector is well-studied, experiments on the laser test facility are operated to investigate the overall reliability of the facility and testing methods. In this experiment, the laser intensity and the voltage of the drift tube detector are fixed; only the relative position of laser focus inside the detector is changed. If the time-over-threshold of the signals has clear dependence on the distance from the laser focus to the anode wire, then it can be proven that the majority number of electrons by primary ionizations are limited within a tiny volume.

The laser repetition rate is set to 10 Hz to avoid saturation effect while having enough statistics. The working gas is 70% Ar + 30% CO_2, and the high voltage of the drift tube is 1700 V. During the experiment, the X axis is defined as the direction along the laser beam, the Y axis is the vertical direction along the slit and perpendicular to the anode wire, and the Z axis is defined as the direction along the anode wire. The power of the laser is measured after the detector to ensure that the laser beam is no in touch with the edge.

We define the direction along the anode wire of the drift tube as the X axis, the vertical direction as the Y axis, and the direction along the laser beam as the Z axis. As the first step of the experiment, the rough position of the laser focus is calibrated by making automatic scans along Y and Z directions. A clear parabola shape is found on the dependence of Y or Z positions on the time. The coordinate of (Y, Z), where the time-over-threshold reaches its minimum value, is the rough position of the anode wire and taken as the zero point in the next step.

On the second step of calibration, accurate scans on Y and Z directions are operated, respectively. In the Z scan, the laser focus is placed on the position $Y = Y_0 + 1000\mu m$ to avoid the anode wire. The step length on the Z-axis is 100 µm. Similarly, a Y-axis scan is operated, the Z position is at $Z = Z_0$, and the step length is 100 µm as well. 3000 events are taken on each position to obtain the average value and variation.

The results of the test are shown in Figure 7. A more precise value of the position of the an-

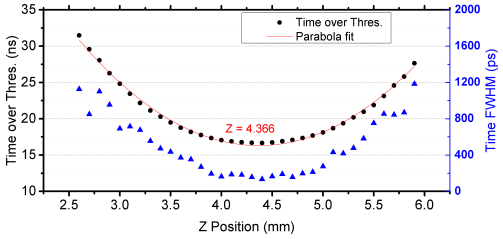

(a) Scan of Z axis when $Y = Y_0 + 1000\mu m$

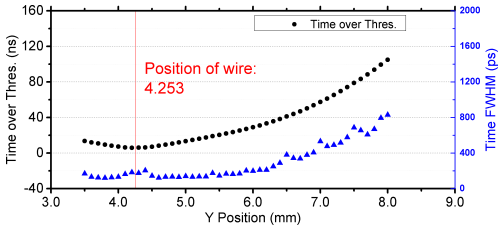

(b) Scan of Y axis when $Z = Z_0$

Figure 7: Time over threshold and time resolution in dependence of the focus position.

ode wire can be obtained by fitting. The FWHM time resolutions of the measurement points increase from 120 to 800 ps as the drift length is increased. The time resolution value is better than the typical value of around 1 ns for drift tube detectors, probably because of the small dimension of the detector and the high position accuracy of the laser. In order to investigate the charge spectrum on a single measurement point, the laser position is set to $(Y = Y_0 + 2000\mu m, Z = Z_0)$ for 10000 events, and the relative deviation of charge is obtained as 5.8%.

If the Y positions are $Y_i, (i = 0, 1, 2, \ldots, n)$ and the time over threshold measured at position Y_i is t_i, then the average electron drift velocity $v_{i.5}$ within the distance is calculated by:

$$v_{i.5} = \left| \frac{Y_{i+1} - Y_i}{T_{i+1} - T_i} \right| . \qquad (13)$$

The electron drift velocity v dependence of the distance to wire is shown in Figure 8 with comparison to a Magboltz simulation. The measurement value of drift velocity is within a 10% difference compare to the Magboltz simulation. Yet

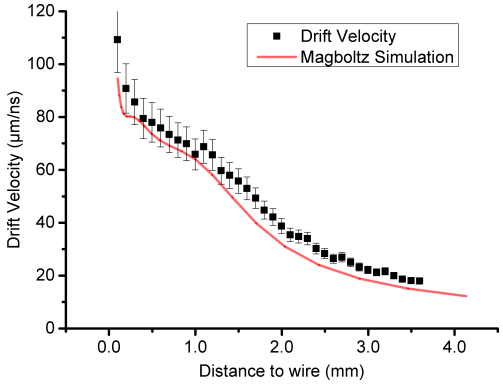

Figure 8: Drift velocity and its comparison to the Magboltz simulation.

when the position is getting closer to the wire, the error becomes larger because the time difference becomes less.

4 Conclusions

The table-size laser test facility in HZDR has reached its initial design goal for micrometer accuracy. With the combination of devices and software, a detailed figure of the spatial distribution of the gaussian-shape laser intensity around laser focus is acquired. The characteristics of multi-photon ionization are investigated with the drift tube detector. The experimental results are in agreement with our simulation works.

The laser test facility is a powerful tool for researches on gaseous detectors. This paper is the first part of the work, as the cornerstone of the fundamental working behaviour of the laser test facility. Further researches related to the precise measurement of gas parameters and investigations for the performance of a gaseous detector will be operated based on the investigations from this work.

Acknowledgement

This study is supported by the European Fund for Regional Development and the Program for

R&D of the Sächsische Aufbaubank under the code WIDDER-100325989.

References

[1] H. Anderhub, M. J. Devereux, and P.-G. Seiler. On a new method for testing and calibrating ionizing particle detectors. *Nucl. Instrum. Methods*, 166(3):581 – 582, 1979.

[2] J. Bourotte and B. Sadoulet. Ionization of Multiwire Proportional Chamber gas by double photon-absorption. *Nucl. Instrum. Methods*, 173(3):463–470, 1980.

[3] H. J. Hilke. On the formation and application of laser-induced ionization tracks in gases. *Nucl. Instrum. Methods*, 174(1-2):145–149, 1980.

[4] J. C. Guo, F. G. Hartjes, and J. Konijn. The use of laser-induced electron clusters for drift chamber tests. *Nucl. Instrum. Methods.*, 204(1):77–83, 1982.

[5] G. Hubricht, K. Kleinknecht, E. Muller, et al. Ionization of counting gases and ionizable gaseous additives in proportional chambers by UV lasers. *Nucl. Instrum. Meth. A*, 228(2-3):327–333, 1985.

[6] H. J. Hilke. Detector calibration with lasers - a review. *Nucl. Instrum. Meth. A*, 252(2-3):169–179, 1986.

[7] A. Colucci, E. Gorini, F. Grancagnolo, et al. Measurement of drift velocity and amplification coefficient in $C_2H_2F_4$-isobutane mixtures for avalanche-operated resistive-plate counters. *Nucl. Instrum. Meth. A*, 425(1-2):84–91, 1999.

[8] G. Chiodini, M. R. Coluccia, E. Gorini, et al. Studies of electron drift velocity and charge spectra in RPC by a UV laser source. *Nucl. Instrum. Meth. A*, 602(3):757–760, 2009.

[9] L. Naumann, M. Siebold, M. Kaspar, et al. Precision measurement of timing RPC gas mixtures with laser-beam induced electrons. *JINST*, 9(10):C10009, 2014.

[10] M. Loeser, M. Siebold, F. Roeser, et al. High energy CPA-free picosecond Yb: YAG amplifier. In *Advanced Solid-State Photonics*, pages AM4A–16.

[11] National Instruments Corporation. Labview user manual.